Instability and Equilibration of Centrifugally Stable Stratified Taylor-Couette Flow

M. Jeroen Molemaker and James C. McWilliams
Institute of Geophysics and Planetary Physics, University of California at Los Angeles, Los Angeles, California 90095-1567

Irad Yavneh
Department of Computer Science, Technion, Haifa, Israel
(Received 4 May 2000)

The flow between two concentric cylinders, $V(r)$, is studied analytically and computationally for a fluid with stable axial density stratification. A sufficient condition for linear, inviscid instability is $d(V/r)^2/dr < 0$ (i.e., all anticyclonically sheared flows) rather than the Rayleigh condition for centrifugal instability, $d(Vr)^2/dr < 0$. This implies a far wider range of instability than previously identified. The instability persists with finite viscosity and nonlinearity, leading to chaos and fully developed turbulence through a sequence of bifurcations. Laboratory tests are feasible and desirable.

DOI: 10.1103/PhysRevLett.86.5270 PACS numbers: 47.20.Ft, 47.20.Ky, 47.55.Hd

The Taylor-Couette problem is the flow between two vertical, rotating, concentric cylinders that are infinitely long. It has a steady, axisymmetric, viscous solution with the azimuthal velocity profile,

$$V(r) = Ar + B/r\,. \tag{1}$$

Here, $A = (r_0V_0 - r_1V_1)/(r_0^2 - r_1^2)$, $B = r_0r_1(r_1V_0 - r_0V_1)/(r_1^2 - r_0^2)$, and $[r, V]_{0,1}$ are the radius and velocity of the inner and outer cylinder, respectively.

A very large number of theoretical and experimental studies of this problem have been performed for fluids with uniform density (e.g., the classic treatise of Chandrasekhar [1], the experimental study of Andereck *et al.* [2], and the survey of Tagg [3]). It is a canonical shear flow that is easily realized in the laboratory, and it is considered a paradigm for transitions in nonlinear dynamical systems.

This paper concerns the Taylor-Couette flow of a fluid with a stable density stratification, which provides a restoring buoyancy force. The study of rotating, stably stratified flows is of particular relevance for geophysical applications, where such flows are widespread due to the earth's rotation and gravity. This problem was first studied by Thorpe [4], who mainly investigated the analogy of the stratified Taylor-Couette flow with the problem of rotating Bénard convection. No further studies on this problem were published until the work of Boubnov *et al.* [5], who investigated experimentally and theoretically the instability of this flow as a model for ocean-flow instabilities. Hua *et al.* [6] studied this problem computationally and reproduced the main features seen in the experiments. Further studies of this problem are reported in Boubnov *et al.* [7,8], and Caton *et al.* [9], whose experiments show a primary bifurcation from an axisymmetric state to an oscillatory state of confined internal waves and a secondary bifurcation with drifting, nonaxisymmetric vortices.

A common feature to all these stratified studies (except Thorpe [4]) is that the outer cylinder is at rest. Recall the famous criterion for axisymmetric, centrifugal instability in an inviscid fluid, originally due to Rayleigh and extended to stratified fluids by Ooyama [10]:

$$\frac{d(Vr)^2}{dr} < 0\,. \tag{2}$$

When the outer cylinder is at rest, this condition is satisfied for any rotation rate of the inner cylinder.

For nonzero viscosity, ν, we can define the Reynolds number,

$$\mathrm{Re} = 0.5(V_1 - V_0)\,(r_1 - r_0)/\nu\,. \tag{3}$$

Finite values of Re stabilize the flow and shrink the unstable regime. Even in the absence of linear instabilities, for large enough values of Re, finite amplitude perturbations can grow and possibly lead to a transition to turbulence [11].

In this Letter, we study stably stratified Taylor-Couette flow which is centrifugally *stable*, i.e., does *not* satisfy (2). No other linear instabilities are known to exist in this regime for unstratified Taylor-Couette flow, e.g., Tagg [3]. Let Ro denote the Rossby number or relative vorticity of the mean flow:

$$\mathrm{Ro} = \frac{r_m\Omega'(r_m)}{2\Omega(r_m)} = \frac{-B}{Ar_m^2 + B}\,, \tag{4}$$

where $\Omega = V/r$ is the angular velocity and r_m is the mean radius. In this paper, we find that all stably stratified, anticyclonic flows ($\mathrm{Ro} < 0$) are linearly unstable. This instability regime includes all flows with $B/A > 0$ as well as the centrifugally unstable regime with $B/A < -r^2$. Since $d(V/r)^2/dr = \mathrm{Ro}4\Omega^2/r$ at $r = r_m$, the centrifugal condition (2) is thus extended to $d(V/r)^2/dr < 0$.

The relative stratification is measured by the Froude number, which is the ratio between rotation and stratification,

$$F = |\Omega(r_m)| \Big/ \sqrt{-\frac{g\,\partial\rho}{\rho\,\partial z}}\,. \tag{5}$$

 0031-9007/01/86(23)/5270(4)$15.00

Here, g is the gravity acceleration and ρ is the density of the fluid. Recall that for stably stratified fluids, $\partial\rho/\partial z < 0$. We also investigate the nonlinear, viscous equilibration of the linearly unstable modes, and find that they are important for a significant range in Re, where laboratory experiments may be feasible.

First, consider the linear stability problem. We summarize here the main results; a more complete report appears in [12]. We start with the inviscid, incompressible Navier-Stokes equations with adiabatically conserved density (except for molecular diffusion, neglected here), where the Boussinesq approximation is employed. These equations are linearized around the vortex solution (1) and a normal-mode perturbation analysis is performed. The perturbation energy balance follows in a straightforward way,

$$dE/dt = -\Omega(r_m)\,\mathrm{Ro}\int\!\!\int\!\!\int_{\mathbf{v}} uv\,d\theta\,dr\,dz\,, \qquad (6)$$

where E is the domain-integrated total (kinetic plus available potential) perturbation energy and u and v are radial and azimuthal perturbation velocities, respectively. Thus, perturbations can grow when their integrated Reynolds stress, $\iiint uv$, is anticorrelated with the mean strain rate, $\Omega(r_m)\,\mathrm{Ro}$.

In the regime where the perturbations are nonaxisymmetric (azimuthal angular wave number $\ell \neq 0$), the relative width of the gap is small [$\epsilon|\ell| \ll 1$, where $\epsilon = (r_1 - r_0)/r_m$)], the stratification is strong ($F \ll 1$), and the flow is anticyclonic ($\mathrm{Ro} < 0$), an explicit solution to the normal-mode problem has been derived [12]. In this regime the exponential growth rate ω of the most unstable mode is

$$\omega \approx -2\,\mathrm{Ro}|\Omega(r_m)\epsilon\ell|e^{2/\mathrm{Ro}}. \qquad (7)$$

Note that the apparent singularity in (7) actually leads to zero growth rates for $\mathrm{Ro} \to 0$. This is related to the fact that for small Ro the interacting Kelvin waves that lead to this instability (as will be discussed later) are exponentially boundary trapped [13]. Equation (7) implies that there are unstable linear modes for all $\mathrm{Ro} < 0$. In the quasigeostrophic limit ($|\mathrm{Ro}| \to 0$), a commonly used approximation for large-scale geophysical flows, the flow is stable, with the growth rate vanishing exponentially fast in Ro (rather than algebraically as might be expected from a regular perturbation expansion about $\mathrm{Ro} = 0$). The optimal growth rate is shown in Fig. 1 as a function of Ro for several values of F. For strong stratification ($F \ll 1$) the growth rate hardly depends on F, consistent with (7). For large values of F, the growth rate behaves linearly with $1/F$; hence it vanishes as the stratification disappears (see [12]). The growth rates in Fig. 1 are for optimal azimuthal and vertical wave numbers l and m. A small band of vertical wavenumbers m allows growth, and this band becomes exponentially small as $|\mathrm{Ro}| \to 0$, centered around the value $m = (\epsilon r_m F\,\mathrm{Ro}\sqrt{\mathrm{Ro}+1})^{-1}$. This implies that in the limits $|\mathrm{Ro}| \to 0$ (no rotation) and $\mathrm{Ro} \to -1$ (pure rotation) the vertical scale is very small compared to the radial scale. Away from these limits the ratio of the vertical scale to the radial scale is $\sim F$. So, for moderate stratification, the vertical and horizontal scales are comparable, whereas for strong stratification the aspect ratio is small.

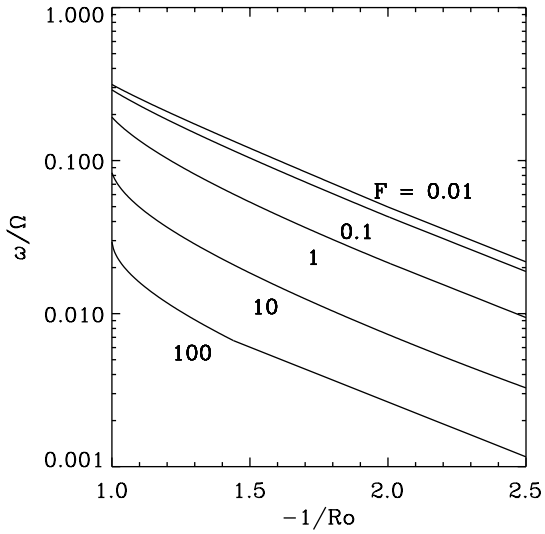

FIG. 1. Inviscid growth rates as a function of Rossby number, for different values of the Froude number. The relative gap width between the cylinders is $\epsilon = 0.1$.

For small viscosity these results remain essentially the same. For all unstable parameter values, such as shown in Fig. 1, there exists a critical value of Re, above which the flow is linearly unstable. In Fig. 2 an unstable eigenmode is shown for $F = 0.01$, $\mathrm{Ro} = -2/3$, and $\mathrm{Re} = 5 \times 10^3$, calculated with the code of [14].

The dynamics of this linear unstable eigenmode can be understood in terms of two boundary-trapped, shear-modified Kelvin waves. Along each wall, the Kelvin waves have a cyclonic propagation tendency due to the rotation and stratification (i.e., moving in an azimuthal direction with the boundary on the right when $\Omega > 0$), which is

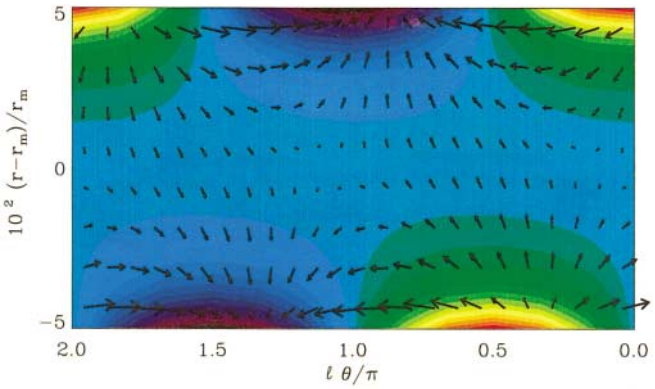

FIG. 2 (color). Eigenmode for $F = 0.01$, $\mathrm{Ro} = -2/3$, $\mathrm{Re} = 5 \times 10^3$, and $\epsilon = 0.1$. Horizontal velocities are shown as vectors, and vertical velocities are shown in color where upward/downward are represented by red/blue, respectively.

arrested by the anticyclonically sheared mean flow. An optimal azimuthal phase shift between the arrested Kelvin waves leads to a u, v correlation that maximizes the growth rate. In [12] unstable higher radial modes of a different nature are reported as well, again for $\mathrm{Ro} < 0$. They are characterized by a weaker growth rate overall with an even steeper exponential decay as $|\mathrm{Ro}|$ decreases. (In the thin-gap limit ($\epsilon|\ell| \ll 1$), the equations of the Taylor-Couette problem reduce to those of a rotating, stratified, uniform-shear channel flow, for which this instability and its mechanism are analyzed in [15]. The phenomenon is related to the wave-wave interaction which is studied in [16].)

Linear instabilities may be "swamped" by nonlinear effects. To establish the relevance of the linear instabilities, we study the finite-amplitude, nonlinear evolution of the linearly unstable flow. The numerical code for these nonlinear calculations is described in [17]. Here we report on the nonlinear equilibration for fixed $F = 0.01$ and $\mathrm{Ro} = -2/3$ as a function of Re in the thin-gap limit, $\epsilon|\ell| \ll 1$. Based on the computations in [12], we expect nearly identical behavior for finite-gap widths such as typically used in experiments (e.g., $\epsilon \approx 0.3$).

A summary of the results is shown in Fig. 3 in the form of a bifurcation diagram [18]. The ordinate shows the extremum of the perturbation vertical velocity, W_{ext}, normalized by the mean azimuthal velocity, V_m.

The flow destabilizes through a pitchfork bifurcation at $\mathrm{Re} \approx 1.1 \times 10^3$. Two symmetry-related branches of stationary stable solutions branch off from this point. Physically, these solutions are equivalent but correspond to a phase shift of $\pi\ell$ in the streamwise direction. The symmetry of the problem is such that if W_{ext} is a solution then $-W_{\mathrm{ext}}$ is also a solution.

In Fig. 4a, stationary solutions along these branches are shown as points in phase space. The ordinate shows

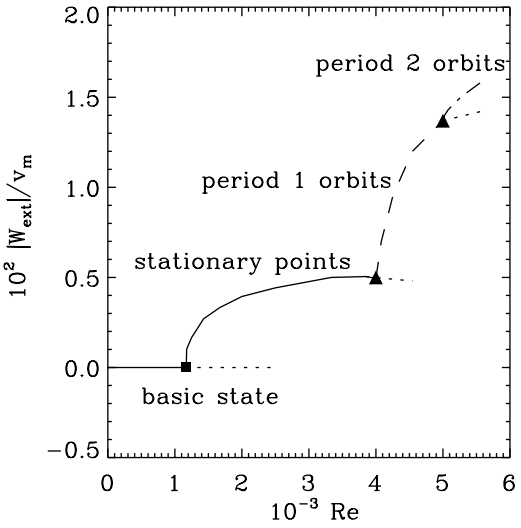

FIG. 3. Bifurcation diagram as a function of the Reynolds number.

the extremum of the normalized, vertical velocity in the lower right quadrant of the domain. It is always located near the boundary. The abscissa shows the phase difference, $\ell\Delta\theta$, between the upper and lower boundary-trapped waves. Near the first bifurcation, the phase difference is close to $\ell\Delta\theta \approx 0.5\pi$, consistent with the physical interpretation of phase-locked Kelvin waves (see Fig. 2) and it decreases for larger values of Re. At a value of $\mathrm{Re} \approx 4 \times 10^3$, the stationary solution loses its stability to time-dependent perturbations through a supercritical Hopf bifurcation. For $4 \times 10^3 < \mathrm{Re} < 5 \times 10^3$, stable limit cycles are found. In Fig. 4b, a phase-space representation of a stable limit cycle for $\mathrm{Re} = 4.9 \times 10^3$ is shown. We start the description of this cycle at the point where the amplitude is small and the phase difference is close to $\ell\Delta\theta \approx 0.5\pi$. At this point the perturbation pattern is very similar to the pattern of the unstable linear eigenmode (Fig. 2). From here the perturbation amplitude grows approximately exponentially by the dynamics of the linear instability [with the growth rate of Eq. (7)]. In the high-amplitude phase of the cycle, the perturbation deforms from the pattern of the linear mode and $\Delta\theta$ decreases. Consequently, the u, v correlation decreases, and the energy transfer from mean flow to perturbation decreases [see Eq. (6)]. Hence, the perturbation amplitude decreases by viscous dissipation. During the small-amplitude phase of the cycle, the sheared mean flow is again able to arrest the Kelvin wave propagation, and the perturbation pattern rearranges into a more favorable phase difference for growth in the next cycle.

At $\mathrm{Re} \approx 5 \times 10^3$ the limit cycles lose their stability through a period doubling or *flip* bifurcation. An example of this period-2 orbit is shown in Fig. 4c. Similar to the period 1 cycle, amplitude growth coincides with a phase difference of $\ell\Delta\theta \approx 0.5\pi$. However, after the interval of increasing $\Delta\theta$ and decreasing growth, instead of returning to this phase difference, the upper and lower extrema now "exchange partners" by continuing their movement in the azimuthal direction, leading to a phase-shifted repeat of the growth-decay cycle. This period-2 cycle therefore "encircles" the two symmetry-related period-1 orbits from Fig. 4b. For even larger Re values, the period-2 orbit becomes unstable to small scale perturbations near the wall and the equilibrated flow behaves more chaotically. We anticipate that, for $\mathrm{Re} \to \infty$, a fully developed turbulent flow will occur with boundary layers near the wall, as previously found in turbulent Couette flow, with and without background rotation [19,20].

These results show that for a significant range in Re the linear eigenmode pattern and its dynamics remain important. This is dramatically different from the cyclonic counterpart of this flow regime (i.e., $\mathrm{Ro} > 0$), where the instability due to Kelvin wave arrest and interboundary phase locking is absent. In the cyclonic, centrifugally stable regime, there are no known linear instabilities, and a transition to turbulence occurs only by nonlinear growth

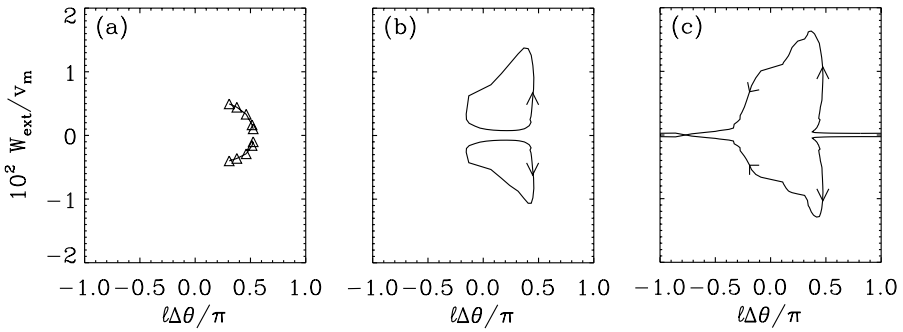

FIG. 4. Phase-space plots of solutions. The horizontal axis is the phase difference between the upper and lower boundary-trapped waves. The vertical axis is the normalized W_{ext} in the lower right quadrant of the domain. (a) Stationary solutions for $1.2 \times 10^3 < \text{Re} < 4.0 \times 10^3$. (b) Period 1 orbit for $\text{Re} = 4.9 \times 10^3$. (c) Period 2 orbit for $\text{Re} = 5.7 \times 10^3$.

of finite-amplitude perturbations at sufficiently high Re values [20]. The value of Re required to obtain nonlinear growth in cyclonic flow is much larger than the range of Re studied here.

This newly discovered Taylor-Couette instability is quite different from other known instabilities in rotating, stratified shear flows. It is not present in unstratified flow. It does not occur in the quasigeostrophic limit, and it is nongravitational and noncentrifugal. It could potentially be of importance to geophysical flows: it occurs in a relevant regime of Ro and Re, and it involves the interaction of shear and inertia-gravity waves, both of which are ubiquitous. Whether the instability is generic to this regime, though, depends on how essential the role of boundaries is. The unstable regime is accessible to laboratory experiments that could both verify our predictions and further develop a different paradigm for transition to turbulence in a canonical shear flow.

Support for this research was provided by the National Science Foundation through the National Center for Atmospheric Research, the Office of Naval Research through Grant No. ONR N00014-98-1-0165, and the Technion V.P.R. Fund for the Promotion of Sponsored Research.

[1] S. Chandrasekhar, *Hydrodynamic and Hydromagnetic Stability* (Dover, New York, 1961).
[2] C. D. Andereck, S. S. Liu, and H. L. Swinney, J. Fluid Mech. **164**, 155 (1986).
[3] R. Tagg, Nonlinear Sci. Today **4**, 1 (1994).
[4] S. A. Thorpe, *Notes on 1966 Summer Geophysical Fluid Dynamics* (Woods Hole Oceanographic Institute, Woods Hole, MA, 1966), p. 80.
[5] B. M. Boubnov, E. B. Gledzer, and E. J. Hopfinger, J. Fluid Mech. **292**, 333 (1995).
[6] B. L. Hua, S. Le Gentil, and P. Orlandi, Phys. Fluids **9**, 365 (1997).
[7] B. M. Boubnov, E. B. Gledzer, E. J. Hopfinger, and P. Orlandi, Dyn. Atmos. Oceans **23**, 139 (1996).
[8] B. M. Boubnov and E. J. Hopfinger, Fluid Dyn. **32**, 520 (1997).
[9] F. Caton, B. Janiaud, and E. J. Hopfinger, Phys. Rev. Lett. **82**, 4647 (1999).
[10] K. Ooyama, J. Atmos. Sci. **23**, 43 (1966).
[11] J. Guckenheimer and A. Mahalov, Phys. Rev. Lett. **68**, 2257 (1992).
[12] I. Yavneh, J. C. McWilliams, and M. J. Molemaker, J. Fluid Mech. (to be published).
[13] J. Pedlosky, *Geophysical Fluid Dynamics* (Academic Press, New York, 1987).
[14] M. J. Molemaker and H. A. Dijkstra, J. Phys. Oceanogr. **30**, 475 (2000).
[15] P. J. Kushner, M. E. McIntyre, and T. G. Shepherd, J. Phys. Oceanogr. **28**, 513 (1998).
[16] S. Sakai, J. Fluid Mech. **202**, 149 (1989).
[17] M. J. Molemaker and J. Vila Guerau de Arellano, J. Atmos. Sci. **55**, 568 (1998).
[18] J. Guckenheimer and P. Holmes, *Nonlinear Oscillations, Dynamical Systems, and Bifurcations of Vector Fields* (Springer, New York, 1983).
[19] O. Dauchot and F. Daviaud, Phys. Fluids **7**, 335 (1994).
[20] K. H. Bech, and H. I. Andersson, J. Fluid Mech. **347**, 289 (1997).